On All Fours: A 3D Framework to Study Closed-loop Control of Quadrupedal Mouse Locomotion

Shravan Tata Ramalingasetty[1], Sergey N. Markin[1], Andrew B. Lockhart [1] Jonathan Arreguit[2], Natalia A. Shevtsova[1], Auke J. Ijspeert[2], Ilya A. Rybak[1], Simon M. Danner[1]

[1]Department of Neurobiology and Anatomy, College of Medicine, Drexel University, Philadelphia, PA, USA
[2]Institute of Bioengineering, École Polytechnique Fédérale de Lausanne, Switzerland
shravantr@gmail.com

Abstract

Quadrupedal locomotion arises from a complex interplay between spinal neuronal circuits, descending brain signals, musculoskeletal interactions, and sensory feedback, enabling adaptive speed and terrain-dependent gait transitions. However, the underlying neural mechanisms involved in limb coordination are poorly understood. Here, we present a proof-of-concept 3D closed-loop neuromechanical model of a mouse that can be used to study interactions between the spinal circuitry and afferent feedback and their role in limb coordination during quadrupedal locomotion. The spinal circuit model includes four rhythm generators, each controlling one limb, that define the locomotor frequency and flexor–extensor alternation. The rhythm generators control pattern formation circuits that generate muscle synergies and create muscle-specific activation patterns. Commissural and long propriospinal interneurons mediate (fore-hind and left-right) interlimb coordination. Afferent feedback (muscle spindle Ia and II, Golgi tendon Ib, and cutaneous) signals interact with the rhythm generators (affecting the timing of phase-transitions), the pattern formation circuits (affecting muscle synergies), and directly with the motoneurons and premotor interneurons, forming basic reflex circuits. Motoneurons activate the muscles to generate locomotor behaviors. Using evolutionary strategies, the model was successfully optimized to locomote over flat ground at different speeds. Acute removal of feedback caused the model to fall and illustrates the capabilities of the model to study neural manipulations. We envision this neuromechanical mouse model to serve as an open testbed to study neural mechanisms for control of complex locomotor behavior in 3D environment.

Introduction

Locomotion is one of the most essential behaviors, by which animals navigate within their environment. In legged animals, locomotion draws together aspects of planning, balance, and coordinated limb movements to adjust for irregular and uneven terrains often encountered in nature. The underlying neural control is a result of the complex interplay between the executive spinal locomotor circuitry, supraspinal commands, inputs from somatosensory afferents, the biomechanics, and the environment. A closed-loop neuromechanical would help to delineate and explore these complex interactions.

Recent advancements in mouse molecular genetics have shed light on the organization and function of spinal and brainstem locomotor circuitry(Kiehn, 2016). Specific neural subtypes have been identified and associated with specific locomotor aspects such as speed-dependent interlimb-coordination (Talpalar et al., 2013; Bellardita and Kiehn, 2015; Kiehn, 2016; Zhang et al., 2022; Ruder et al., 2016), and descending control of locomotor speed, initiation, and stopping (Capelli et al., 2017; Caggiano et al., 2018; Josset et al., 2018; Bouvier et al., 2015; Leiras et al., 2022). Furthermore, targeted manipulation of proprioceptive feedback (Akay et al., 2014; Mayer et al., 2018), and of neuron classes mediating afferent feedback (Gradwell et al., 2024; Laflamme et al., 2023) has yielded novel insights into sensorimotor processing during locomotion (Frigon et al., 2021). Yet, underlying mechanisms including circuit organization and function and the dynamic interactions between individual components are difficult to capture with experimental methods alone and the challenge still remains in being able to manipulate and record multiple centers of the locomotor systems simultaneously. Conducting animal experiments are further complicated because of ethical considerations and long time frames involved in animal preparations.

Computational models of animal locomotion offer a complementary paradigm to test and investigate locomotor systems and alleviate some of the challenges posed by direct animal experiments. Indeed, computational models of spinal locomotor circuitry have not only reproduced experimental findings, but were also instrumental in identifying potential neural mechanisms and organization of the brainstem and spinal locomotor circuits (Rybak et al., 2015; Danner et al., 2016, 2017; Ausborn et al., 2019, 2021). In parallel, neuromechanical models have provided insight into the role of afferent feedback in control of locomotion (Yakovenko, 2011; Ekeberg and Pearson, 2005; Aoi et al., 2013; Kim et al., 2022; Toeda et al., 2020). This further illustrates that in order to study neural control of locomotor behavior it is essential to simulate the mouse biomechanics and its physical environment.

Here, we present a proof-of-concept 3D neuromechanical

model of mouse locomotion that integrates a detailed neural network model of the spinal locomotor circuitry with a quadrupedal musculoskeletal model of the mouse (Figure **??**). The neural-biomechanical interactions enabled the model to stably locomote using a trot gait. We show exemplary simulations of neural manipulations. Specifically, we show that the removal of afferent feedback connections causes the model to lose stability and fall. Such simulations can be used in the future to perform neural manipulations and explore interactions between the spinal circuits and somatosensory feedback in the control of open field 3D quadrupedal locomotion. The components of the simulation framework are being developed to be an open-source project, allowing for replication and improvements to the mouse model in the future.

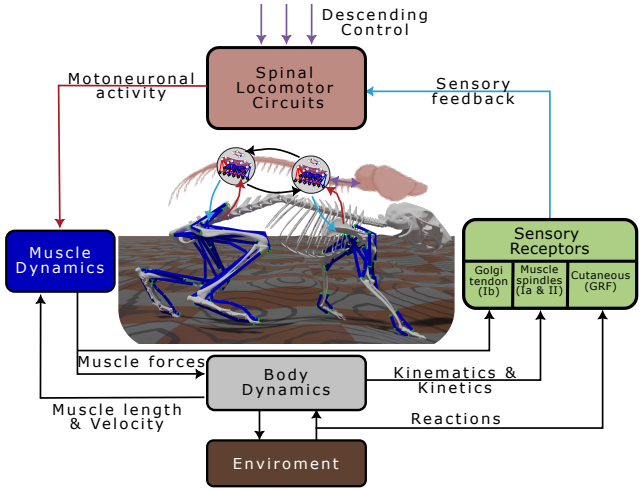

Figure 1: Components of the 3D mouse neuromechanical model to simulate closed loop locomotion. The spinal locomotor circuitry consists of neural models of rhythm generating, pattern formation, motoneurons and low level reflexes. Descending drive activates and modulates the locomotor circuitry. Motoneural activity serves as input to the muscle models, which in turn produce appropriate muscle forces defined by Hill-type muscle dynamics. The body responds to the muscle forces to produce movement by interacting with the environment. Computed proprioceptive (muscle spindles and golgi tendon organs) and exteroceptive (cutaneous receptors) is fed back to the spinal circuitry, interacting with it at all levels. This figure has been adapted from Paul et al. (2005) and the brain-spinal cord graphic created with BioRender.com.

Related Works

Computational models of spinal circuitry

Computational models of spinal locomotor circuitry have progressively been extended to accommodate and explain experimental findings as they became available (Rybak et al., 2015; Danner et al., 2016, 2017; Ausborn et al., 2019, 2021). Spinalized animal preparations have shown that the neural circuitry located in the spinal cord is sufficient to produce basic locomotor-like rhythmic activity. Indeed, it has been shown that neural networks in the spinal cord, termed central pattern generators or rhythm generators, are capable of producing rhythmic motor output even when isolated from supraspinal inputs and afferent feedback. The model of half-center rhythm generator effectively elucidated the central regulation of alternating flexion-extension muscle activity. However, it fell short in accounting for the intricacies of more complex motor patterns, such as spontaneous deletion of motor activity. Subsequently, the development of a two-layered network, comprising a rhythm generator and a pattern formation layer, proved capable of successfully reproducing these observations seen in fictive spinal preparations (McCrea and Rybak, 2008). Subsequent genetic identification of spinal interneurons involved in speed-dependent gait expression in mice (Bellardita and Kiehn, 2015) led to models investigating central neural interactions between rhythm generators controlling individual limbs (Danner et al., 2017; Zhang et al., 2022). However, these detailed neural network models did not consider sensory feedback, which interacts with the spinal locomotor circuitry and plays a crucial role in shaping motor patterns during locomotion in intact animals.

Musculoskeletal models of mice

Developing detailed musculoskeletal models is a challenging endeavor. It involves simulating the mechanics of articulated rigid bodies, their interactions with the environment, and the dynamic forces generated by muscles. Charles et al. (2016a,b) developed a detailed musculoskeletal model of a single hindlimb of the mouse in OpenSim (Seth et al., 2018). Charles et al. (2018), later used the musculoskeletal model to directly estimate the muscle activity necessary for trotting using a quasi-static optimization technique. Tata Ramalingasetty et al. (2021) built a whole-body musculoskeletal model of the mouse by combining data from Charles et al. (2016a) for the hindlimbs and data from DeLaurier et al. (2008) for the forelimbs. Merel et al. (2019) developed a detailed mouse musculoskeletal model to simulate full 3D locomotion. However, this model used a more abstract description for musculature consisting of only simple flexor-extensor muscles.

Neuromechanical simulations

Most neuromechanical simulations employ *biologicaly inspired* controllers to drive the musculoskeletal model. However, neuromechanical simulations often end up with a high number of open parameters that makes answering specific scientific questions challenging. A common approach to address this problem is to abstract away open parameters that are not within the focus of the study. This methodol-

ogy provides more tractable simulations. Ekeberg and Pearson (2005) aimed to study the role of ankle loading and hip stretch feedback in the hindlimbs during locomotion in cats. They used a state-machine to represent the nervous system that generated phase-dependent muscle activity. The study highlighted key differences in the relative importance of two complementary feedback pathways. Toeda et al. (2020) developed a neuromechanical simulation of a rat to investigate speed-dependent gait changes. The authors presented an abstract representation of the two-layered locomotor network to generate phase-dependent muscle activity based on muscle synergies. Saputra et al. (2020, 2022) built a neuromechanical model of the dog with neural network based on the principles of a two-layered locomotor network. Geijtenbeek et al. (2013) highlights the power of neuromechanical simulations by generating arbitrary animal configurations that can successfully locomote. Overall, previous neuromechanical simulations of quadrupedal locomotion have been isolated, independent bodies of work.

In this work, we focused on each of the subcomponents of the mouse neuromechanical simulation. In order to study sensory feedback, it is essential to simulate the musculoskeletal system. We extended the neural model presented in Zhang et al. (2022) with pattern formation and motor neuron layers. Additionally, we connected the proprioceptive and somatosensory feedback to all levels of the network.

Methods

Musculoskeletal system

The musculoskeletal model described in this paper is a simplified version of the whole-body mouse musculoskeletal model developed by Tata Ramalingasetty et al. (2021). Specifically, we modeled groups of agonist muscles as single muscles and reduced the degrees of freedom (DoF) of the spine.

Skeleton: In the current description of the skeletal system, a joint can consist of one or more DoF with the same center of rotation. The skeletal system consisted of 17 joints with 25 DoF in total. Each hindlimb had a 3-DoF hip joint, 1-DoF knee, ankle and meta-tarsal joints. Each forelimb had a 3-DoF shoulder joint, 1-DoF elbow, and wrist joints. The spine was modeled as three joints: lumbar, thoracic and cervical joints with 1 DoF each (midsagittal flexion/extension). Joint movements in the hindlimbs and forelimbs were actively controlled by the limb muscles while joints in the spine were passive and actuated as spring-damper systems. For small movements, the spine would correspond to tonically activated muscles to provide the necessary compliance for quadrupedal locomotion. Figure 2 highlights the locations of the joints in the mouse skeletal system.

Muscles: Muscles are force-generating elements that receive inputs from the neural circuitry and generate forces based on muscle fiber contraction dynamics. We modeled major flexor and extensor muscles as well as adductor and abductor muscles for both forelimbs and hindlimbs. The muscle's contraction dynamics was modeled using three-element Hill-type muscles (De Groote et al. (2016); Figure 3) with stiff tendons. Similarly to the mouse model in Tata Ramalingasetty et al. (2021), muscle paths were approximated as a series of linear segments that wrap around joints.

The hindlimbs of the model include 12 muscle-tendon units (MTUs), categorized into 8 uniarticular muscles: Iliopsoas (**IP**) for hip flexion, Biceps Femoris Anterior (**BFA**) for hip extension, Adductor Brevis (**AB**) for hip adduction, Gluteus Maximus (**GM**) for hip abduction, Rectus Femoris (**RF**) and Vastus Lateralis (**VA**) for knee extension, Tibialis Anterior (**TA**) for ankle dorsiflexion, Soleus (**SOL**) for ankle plantarflexion; and 4 biarticular muscles: Biceps Femoris Posterior and Semitendinosus (**BFPST**) for hip extension and knee flexion, Medial Gastrocnemius (**MG**) for knee flexion and ankle plantarflexion, Extensor Digitorum Longus (**EDL**) for ankle dorsiflexion and metatarsophalangeal extension, and Flexor Digitorum Longus (**FDL**) for ankle plantarflexion and metatarsophalangeal flexion.

The forelimb contains 10 MTUs: 9 uniarticular muscles, including Supraspinatus (**SSP**) for shoulder protraction, Spinodeltoideus (**SPD**) for shoulder retraction, Adductor (**ADD**) for shoulder adduction, Abductor (**ABD**) for shoulder abduction, Triceps Brachii Long Head (**TBO**) for elbow extension, Biceps Brachii Short Head (**BBS**) and Brachialis (**BRA**) for elbow flexion, Extensor Indicis Proprius (**EIP**) for wrist dorsiflexion, Flexor Carpi Ulnaris (**FCU**) for wrist plantarflexion, and 1 biarticular muscle, Triceps Brachii Lateral Head (**TBL**), serving both shoulder retraction and elbow extension functions.

In total, the model comprised of 44 MTUs controlling 25 DoFs within the hind and forelimbs to produce locomotor movement.

Neural system

The model of the spinal neural circuitry controlling the musculoskeletal system of the mouse is based on recent models of central control of interlimb coordination (Danner et al., 2017; Zhang et al., 2022) and the two level central pattern generator described in McCrea and Rybak (2008). The circuitry was modeled as a network of interconnected neuronal populations. Individual neuronal populations were modeled as non-spiking, activity-based leaky integrator neuron population models Ermentrout (1994); Danner et al. (2017). Neuronal populations of excitatory rhythm generation and pattern formation centers included a slowly-inactivating persistent sodium current (I_{NaP}).

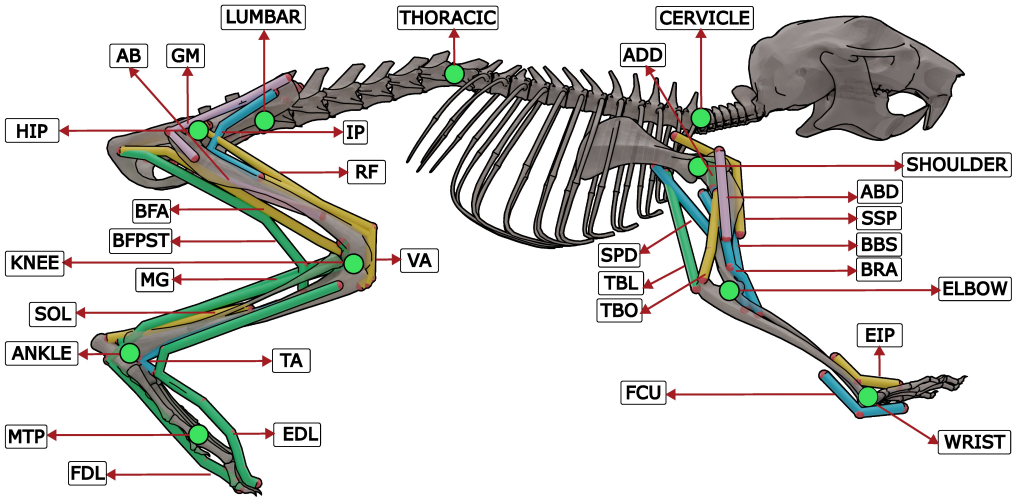

Figure 2: Musculoskeletal system with highlighted hind and forelimb musculature and joints. Joints are highlighted as ■. Extensor muscles are represented by the color ■, flexor muscles by ■ and biarticular muscles by ■. For visual clarity, only the right limbs are shown.

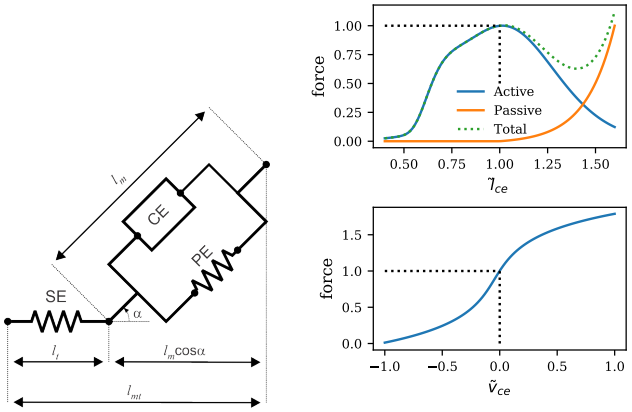

(a) (b)

Figure 3: Hill-type muscle model (a) and its dynamics. The contractile element (CE) models the force-length and force-velocity relationship shown in (b). The parallel element (PE) prevents the muscle from overstretching beyond its normal range of operation. The series element (SE) models the series elasticity of the muscle-tendon unit. l_{mt} represents the muscle-tendon unit length, l_m is the length of the muscle fiber, α_0 is the default pennation angle and l_t is the tendon length. Figure reproduced from Tata Ramalingasetty et al. (2021)

Central or feedforward network

The spinal circuit model includes four rhythm generators, each controlling one limb, that define the locomotor frequency and flexor–extensor alternation (Shevtsova et al., 2015; Danner et al., 2016)(Figure 4a). The rhythm generators control pattern formation circuits to transform neuronal activity into muscle synergies and create muscle-specific activation patterns. The pattern formation layer produces four basic patterns; two patterns during flexion phase and two patterns during the extension phase. Motoneurons then receive a weighted combination of select patterns and activate corresponding muscles to generate locomotor behaviors (Figure 4b). A global drive simulates the effects of descending control signals from the brainstem. Excitatory brainstem drive to the rhythm generation and pattern formation centers controls frequency and amplitude of synergies, respectively. Finally, interlimb coordination (fore–hind, left–right, diagonal) is controlled by commissural and long propriospinal interneurons that mediate interactions between the four rhythm generators (Danner et al., 2017; Zhang et al., 2022)(Figure 4a).

Feedback connectivity

Proprioceptive feedback from the muscles and cutaneous feedback from the plantar surface of the paws were calculated from the musculoskeletal model and influenced the spinal locomotor circuitry at all levels. This formed a closed-loop system with the inclusion of the mouse musculoskeletal system and the physical environment. Afferent feedback consisted of muscle spindle Ia and II, Golgi tendon Ib, from each muscle-tendon unit and cutaneous feedback from the plantar surfaces of the hind and fore paws. Muscle spindles Ia and II measure muscle length and velocities, while the Golgi tendon Ib afferent measures the force generated by the muscle and were calculated by the equations described in (Prochazka and Gorassini, 1998; Prochazka, 1999; Markin et al., 2010). Cutaneous feedback measured the ground reaction forces when the foot interacts with the ground. Feedback signals were connected to the rhythm generation level (affecting the timing of phase-transitions), to the pattern formation circuits (affecting muscle synergies), and directly to motor neurons and premotor interneurons, forming basic reflex circuits.

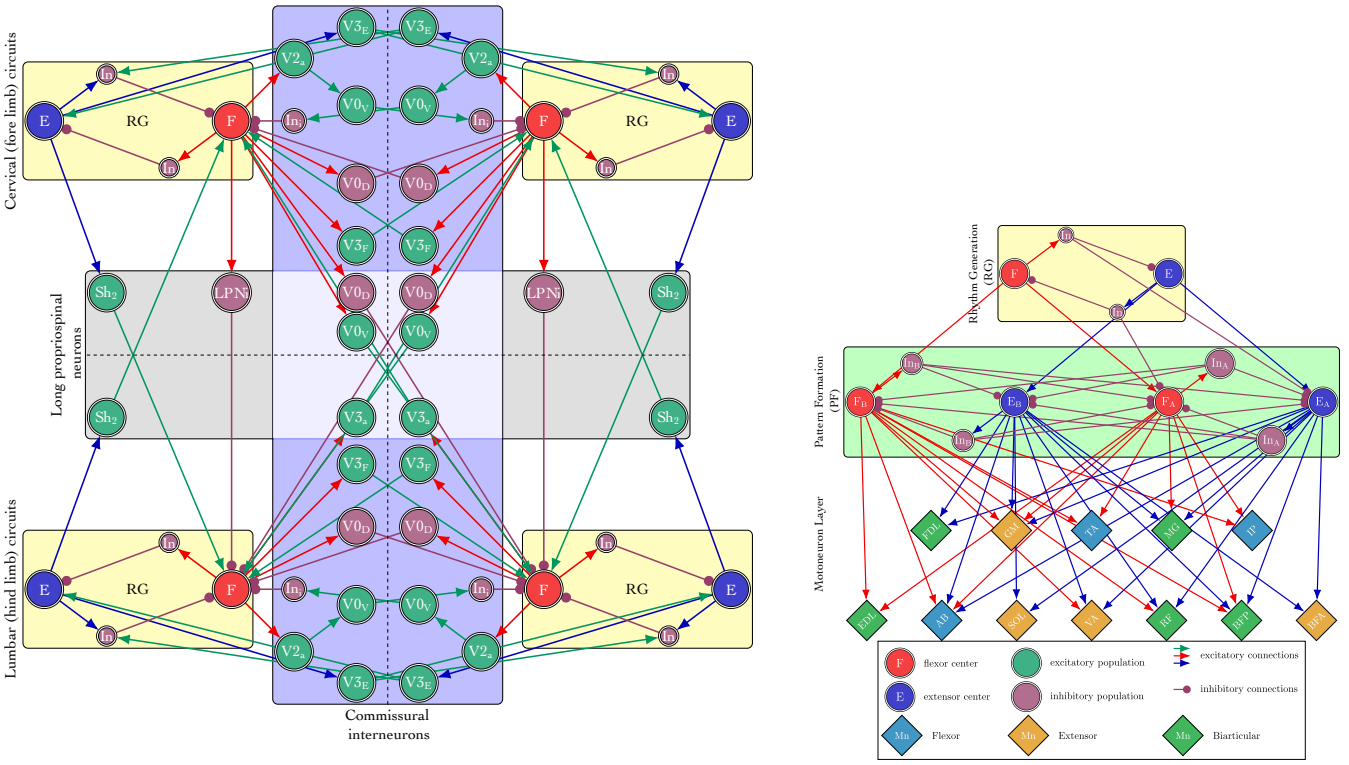

(a) (b)

Figure 4: Connections within the spinal circuitry model. Each node/circle represents a neural population of neural type in the spinal cord; excitatory and inhibitory connections are marked by arrowheads and circles, respectively. (a) four rhythmn generators (RGs; each controlling one limb) and connections between them through commissural and long propriospinal neurons. (b) two-layer network for each limb, with RG centers of (a) connected to a pattern formation layer which then projects to the motoneuron layer that excite the limb muscles.

Feedback to the rhythm generation and pattern formation centers: The rhythm generators received muscle spindle, golgi tendon and cutaneous feedback affecting timing of phase-transitions (Schomburg et al., 1998; Fujiki et al., 2019; Kim et al., 2022). Group II spindle feedback of hip (iliopsoas) and ankle flexors (tibialis anterior) of the hindlimb, or shoulder (supraspinatus), elbow (brachialis) and wrist (extensor indicis proprius) flexors of the forelimb were connected to the respective flexor centers as well as the inhibitory interneurons inhibiting the extensor centers. These connections will promote a transition of stance to swing when the respective limb is hyperextended, as described experimentally for the hindlimbs (Hiebert et al., 1996; Ekeberg and Pearson, 2005; Rossignol et al., 2006).

Ib Golgi tendon feedback of ankle (medial gastrocnemius, soleus) and metatarsal (flexor digitorum longus) extensors of the hindlimb and wrist extensors (flexor carpi ulnaris) of the forelimb were connected to the extensor center and the inhibitory interneuron inhibiting the flexor center of the respective rhythm generators. Cutaneous feedback from the plantar surface of each foot was connected to the extensor center and inhibitory interneuron inhibiting the flexor center of the same limbs rhythm generator. These connects promote a prolongation of extension phase when the leg is not unloaded during stance (Guertin et al., 1995; Whelan et al., 1995; Whelan and Pearson, 1997; Rossignol et al., 2006).

Group II spindle feedback from hip (iliopsoas), ankle (tibialis anterior) and metatarsal (extensor digitorum longus) flexors of the hindlimb, and shoulder (spinoltoideus) and wrist (extensor indicis proprius) flexors of the forelimb were connected to the respective flexor and extensor centers of the pattern formation layer.

Low level reflexes: Basic low-level reflex circuits are organized according to well-established literature (Pierrot-Deseilligny and Burke, 2012) and include Ia monosynaptic excitation of homonymous motoneurons, Ia reciprocal inhibition, as well as Ib disynaptic inhibition and excitation. Specifically, monosynaptic Ia excitation was modeled by connecting Ia feedback of each muscle to its own motorneuron. In the case of reciprocal inhibition, Ia feedback from extensor motoneurons inhibited their antagonist flexor muscle motor neurons through an inhibitory interneuron, and vice versa for flexor Ia feedback inhibiting their antagonist extensor muscle motor neuron. Furthermore, Ib disynaptic inhibition feedback was modeled by connecting Ib feedback from each muscle to an inhibitory interneuron which then inhibits the homonymous motoneuron. Similarly, Ib disy-

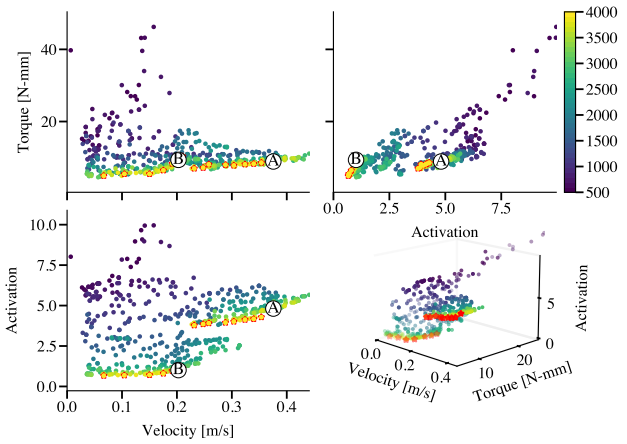

Figure 5: Evolution of multi-objective optimization along the three objectives (speed, torque, and muscle activation's) over the generations (indicated by the colorbar) represented as a pairwise relationship between two objectives. The solution set characterized by red stars highlights the Pareto front obtained from the final 4000$^{\text{th}}$ generation. Marked **A** and **B** on the Pareto front represent the two solutions picked for further analysis.

naptic excitation was mediated by excitatory interneurons and included only for anti-gravity muscles. Additionally, the model incorporates recurrent inhibition and reciprocal facilitation mediated by Renshaw cells.

Simulation

The closed loop neuro-mechanical interactions were simulated in a 3D physics environment with MuJoCo Todorov et al. (2012) under the FARMS Arreguit et al. (2024) simulation framework. A simulation is run for 8 seconds at 1-milli-second timesteps for the integration of the physics and the neural network.

Optimization

We used a multi-objective covariance matrix adaptation-evolution strategy (CMA-ES) Hansen et al. (2019); Hansen and Ostermeier (2001) to identify open model parameters (descending drives, muscle synergy weights, and feedback weights) that lead to stable locomotion. It is common practice to formulate a single objective optimization as a weighted sum of different objectives (Geijtenbeek et al., 2013). Yet, animals find different trade-offs to complete the necessary task, leading to a diverse set of behaviors. Or the trade-offs are simply not known and or would require *a priori* knowledge of the expected outcomes and could lead to biased solutions depending on the weighting.

On the other hand, in a multi-objective formulation, the optimizer algorithm attempts to find a set of solutions that are trade-offs between the different objectives (Arreguit et al., 2021). The solution set of interest is the Pareto-front. A solution is considered to be part of the Pareto-front if there exists no other solution which dominates it over the set of objectives.

In this work, the objectives of the optimizer were to maximize the average velocity, and minimize the cumulative torques and squared muscle activations during the simulation. The optimization was subjected to a set of constraints that had to be satisfied. These included maintaining a minimum pelvis and head height, not engaging ligament forces, and avoiding knee and heel contacts with the ground during locomotion. In the solution set, all penalties were eliminated. The decision vector for the multi-objective CMA-ES optimizer included network weights connecting the pattern formation layer and the motor neurons, all feedback weights. The multi-objective optimization was thus formulated as,

$$\text{Minimize} \quad f_1(\mathbf{x}) = -d_{\text{forward}} \tag{1}$$

$$f_2(\mathbf{x}) = \frac{1}{T}\sum_{t=0}^{t=T}\sum_{j=0}^{j=N} \|\tau_j(t)^2\| \tag{2}$$

$$f_3(\mathbf{x}) = \frac{1}{T}\sum_{t=0}^{t=T}\sum_{m=0}^{m=K} A_m(t)^2 \tag{3}$$

$$\text{Subject to} \quad Z_{pelvis} > 0.015 \tag{4}$$

$$\sum_{j=0}^{j=N} \mathbf{F_j} = 0.0 \tag{5}$$

Constraints described in equations 4, 5 are added to each objective as penalties to formulate a constrained optimization problem.

In this formulation, d_{forward} is the distance walked by the model over a simulation of duration T seconds, $\tau_j(t)$ designates the torque of joint j at time t, $A_m(t)$ is the activation of muscle m at time t, Z_{pelvis} is the height of the pelvis which is constrained to be over a height of 1.5 [cm], and $\mathbf{F_j}$ are the joint limit forces.

Results

Using the multi-objective CMA-ES algorithm, spinal locomotor circuit parameters were evolved to generate a population of solutions that successfully locomoted on all four limbs (Figure 8).

Figure 5 illustrates the progress of the optimization process over 4,000 generations with a population size 24, starting from a set of solutions obtained by sampling the decision vector from a random normal distribution. The Pareto front (highlighted as red stars in Figure 5) shows the conflicting nature of the three objectives (velocity, torques and squared muscle activation). In this case (with three objectives), the Pareto front is a surface (as seen in the 3D scatter plot). Each solution on the Pareto front represents a trade-off between the three objectives at the time of the final generation (4,000). Pairwise plots are useful in observing the relationship between any two pairs of the three objectives. At the

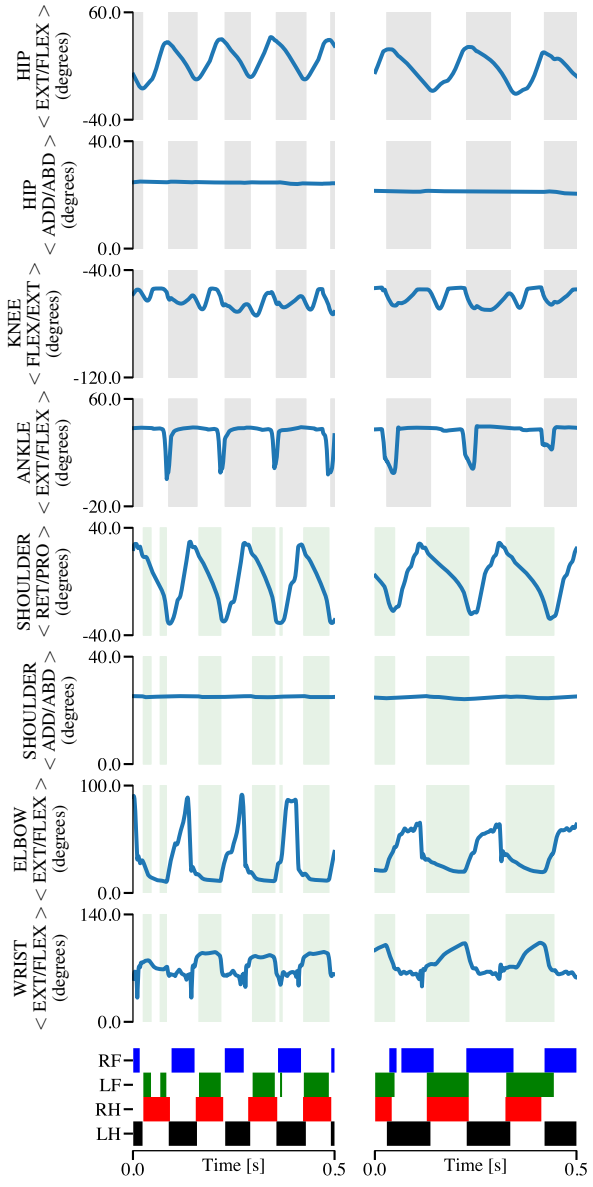

Figure 6: Joint kinematics of left hind and forelimb for two solutions **A** and **B** representing fast (0.375 m/s, left) and slow (0.21 m/s right) speeds from the Pareto-front generating mouse locomotion over flat terrain after optimization. Plots represent 0.5 seconds of simulation time starting at $t = 8.0s$. Ext/Flex represent the flexion-extension joint angles of hip, knee, ankle, elbow and wrist joints, ADD/ABD represent the adduction-abduction joint angles of hip and shoulder joints and ret/pro represent the protraction-retraction joint angles of the shoulder joint. Shaded regions indicate the stance duration of the respective limb. Stances of right fore (RF), left fore (LF), right hind (RH) and left hind (LH) for each solution are shown in the bottom stance plot

time of termination of the optimization algorithm, the relationship between forward velocity and torque, as well as between velocity and activation, demonstrates typical conflicting goals inherent in multi-objective optimizations. However, the relationship between muscle activation and torque exhibits a more complex cluster.

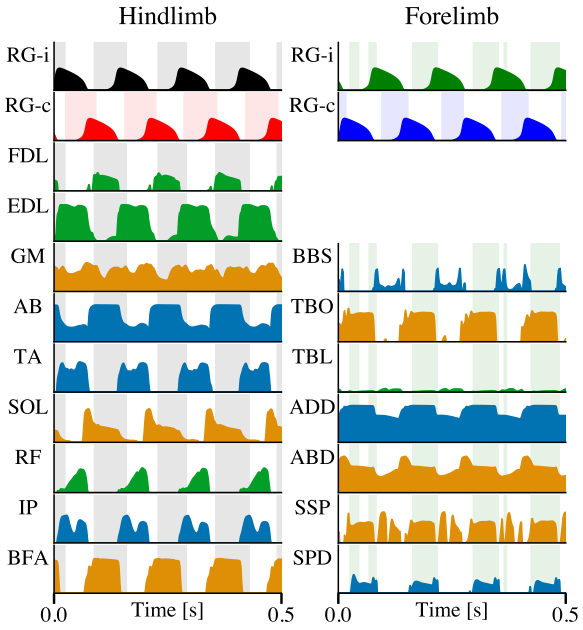

Figure 7: Spinal locomotor circuit model performance during fast lomocotion (0.375 m/s) for 0.5 seconds of simulation time starting at $t = 8.0s$. Interlimb coordination between the four limbs are indicated by the flexor activity of the respective rhythm generation center on the ipsilateral (RG-i) and contralateral side (RG-c). Motoneuron activity for each hindlimb and forelimb muscle for the left side are plotted. Motorneurons that were optimized to have no activation (BFPST, VA and MG in the hindlimb and FCU in the forelimb) are not shown in the plots. Shaded regions in the background indicate the stance phases of the respective limb obtained based on the ground contact during the simulation.

Figure 6 displays the joint kinematics for two specific solutions from the Pareto front (marked **A** and **B** in Figure 5). The two solutions picked exhibit different velocities; one represents a higher velocity (0.375 m/s) with a net torque of 8.9 $N - mm$ and a cumulative muscle activation of 4.81, and the other slower velocity (0.21 m/s) with a net torque of 10.4 $N - mm$ and a cumulative muscle activation of 1.2. For the hip joint, the flexion and extension phases align and adapt with the limbs swing and stance phases. In both cases, hip abduction-adduction and knee flexion-extension were held at a relativaly constant angle. The ankle joint exhibits the biggest difference with the faster solution keeping the ankle joint stiff at a constant angle during both swing and stance phases. For the slower solution, the ankle joint alternates between flexion and extension during swing and stance phases respectively. Similarly to the hip flexion-extension, the shoulder protraction and retraction aligns with the swing and stance phases of

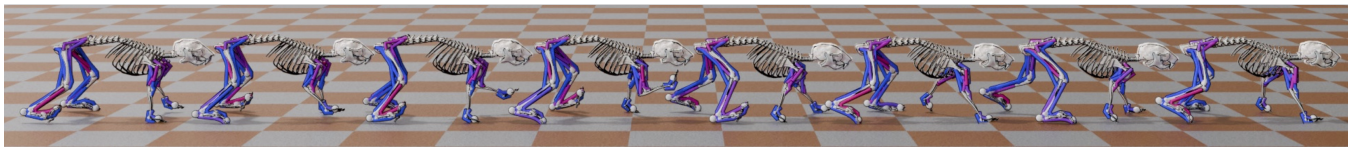

Figure 8: Gait snapshot of the 3D neuromechanical model walking over a flat terrain with the spinal locomotor circuitry and afferent feedback driving the hindlimb and forelimb muscles. Snapshots were taken at an interval of 0.2 seconds.

the forelimb. Shoulder abduction-adduction is held constant throughout the gait cycles. Elbow flexion-extension in both cases have a very similar range of motion and again align themselves with the swing and stance phases of the limb. Wrist flexion-extension has a different range of motion between the speeds but exhibit a similar phasic relationship. Despite these differences, the stance plots indicates that the model consistently prefers trot to maintain stable locomotion at both speeds. The slow speed was achieved by increasing the stance duration while keeping the swing duration relatively constant compared to the faster speed, a typical strategy observed in quadrupedal locomotion.

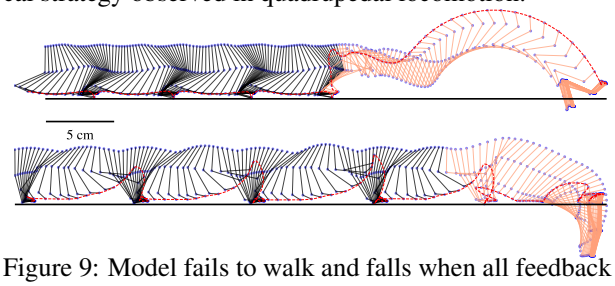

Figure 9: Model fails to walk and falls when all feedback to the spinal circuitry is removed abruptly during locomotion. Kinematics of right hind (top) and forelimb (bottom) represented as stick diagram. Highlighted in black represents the intact case and orange marks the changes in locomotion after the removal of feedback.

To demonstrate the influence of feedback on the spinal locomotor circuitry, we abruptly disconnected feedback (all feedback-connection weights were set to 0) to the spinal locomotor circuit during stable locomotion. In Figure 9, hindlimb and forelimb kinematics are separately represented as stick figures. A stable locomotor regime is shown as black segments and from the moment the feedback was removed is highlighted as orange. As soon as the feedback is removed the model immediately loses stability, falls, and is no longer able to locomote.

Discussions

In this paper, we presented a 3D closed-loop neuromechanical model of a mouse driven by detailed spinal locomotor circuitry and used it to generate stable quadrupedal locomotion at two different speeds. This process involved adapting and combining the mouse biomechanical model developed by (Tata Ramalingasetty et al., 2021) and the computational models of spinal locomotor circuits (Danner et al., 2016, 2017) into a common framework that can interact with each other in a 3D physical environment simulated by MuJoCo physics engine (Todorov et al., 2012). All the components of the simulation were developed and integrated using the FARMS framework (Arreguit et al., 2024).

Extending the central spinal circuitry required addressing important questions about connecting feedback to the central model. The role of the feedback connections presented here and the ones to be considered in the future are all subject to investigation on their influence during locomotion. The current model is a proof-of-concept setup for our upcoming studies on sensorimotor integration in the spinal circuits.

Instead of optimizing the mouse model to generate specific experimentally observed kinematics, we used CMA-ES, an evolutionary optimization algorithm, and the resulting kinematics emerge based on our assumptions on the spinal circuit, biomechanics, and optimization formulation. This methodology provides a powerful way to test our translation of current experimental findings to computational models. However, this is a challenging endeavour and requires continued, iterative development.

Although the model produced stable locomotor gaits at different speeds, it did not result in a physiological range of speeds and gaits—indeed, only trot was expressed by the model. Furthermore, model kinematics, while functional, differ from experimentally observed kinematics. This requires further investigation and model refinement.

The next steps include connecting a model of the vestibular system and descending interactions of vestibular tract neurons with the spinal locomotor circuitry to improve balance and stability of 3D-locomotion and train the model to walk on more diverse terrains such as slopes and hills.

In the future, we will continue to extend our model to simulate control of full 3D-quadrupedal locomotion with the aim of providing an open-source model that can be used as a testbed for exploring different hypotheses related to the interactions between spinal circuits and sensory feedback. The computational model will be made available as an open-source tool and will allow anyone to ask "what-if" questions by challenging neural or biomechanical parameters and observing emergent locomotor behaviors (Allen and Ting, 2016). It will be a valuable tool for the larger community studying various aspects of neural control of locomotion.

Acknowledgements

This study was supported in part by NIH grants R01NS112304, R01NS115900, R01NS100928, and R01NS110550; NSF CR-CNS/DARE grant 2113069; and ERC Salamandra project grant 951477.

References

Akay, T., Tourtellotte, W. G., Arber, S., and Jessell, T. M. (2014). Degradation of mouse locomotor pattern in the absence of proprioceptive sensory feedback. *Proceedings of the National Academy of Sciences*, 111(47):16877–16882.

Allen, J. L. and Ting, L. H. (2016). Why Is Neuromechanical Modeling of Balance and Locomotion So Hard? In Prilutsky, B. I. and Edwards, D. H., editors, *Neuromechanical Modeling of Posture and Locomotion*, pages 197–223. Springer, New York, NY.

Aoi, S., Kondo, T., Hayashi, N., Yanagihara, D., Aoki, S., Yamaura, H., Ogihara, N., Funato, T., Tomita, N., Senda, K., and Tsuchiya, K. (2013). Contributions of phase resetting and interlimb coordination to the adaptive control of hindlimb obstacle avoidance during locomotion in rats: a simulation study. *Biological Cybernetics*, 107(2):201–216.

Arreguit, J., Ramalingasetty, S. T., and Ijspeert, A. (2024). FARMS: Framework for Animal and Robot Modeling and Simulation.

Arreguit, J., Ramalingasetty, T. S., Gupta, A., and Ijspeert, A. (2021). Multi-Objective Optimization based 3D Walking of a Neuromuscular Driven Salamander Model in Simulation. In *Adaptive Motion of Animals and Machines (AMAM)*. Adaptive Motion of Animals and Machines Organizing Committee.

Ausborn, J., Shevtsova, N. A., Caggiano, V., Danner, S. M., and Rybak, I. A. (2019). Computational modeling of brainstem circuits controlling locomotor frequency and gait. *eLife*, 8:e43587.

Ausborn, J., Shevtsova, N. A., and Danner, S. M. (2021). Computational Modeling of Spinal Locomotor Circuitry in the Age of Molecular Genetics. *International Journal of Molecular Sciences*, 22(13):6835.

Bellardita, C. and Kiehn, O. (2015). Phenotypic Characterization of Speed-Associated Gait Changes in Mice Reveals Modular Organization of Locomotor Networks. *Current Biology*.

Bouvier, J., Caggiano, V., Leiras, R., Caldeira, V., Bellardita, C., Balueva, K., Fuchs, A., and Kiehn, O. (2015). Descending command neurons in the brainstem that halt locomotion. *Cell*, 163(5):1191–1203.

Caggiano, V., Leiras, R., Goni-Erro, H., Masini, D., Bellardita, C., Bouvier, J., Caldeira, V., Fisone, G., and Kiehn, O. (2018). Midbrain circuits that set locomotor speed and gait selection. *Nature*, 553(7689):455–460.

Capelli, P., Pivetta, C., Soledad Esposito, M., and Arber, S. (2017). Locomotor speed control circuits in the caudal brainstem. *Nature*, 551(7680):373–377.

Charles, J. P., Cappellari, O., and Hutchinson, J. R. (2018). A Dynamic Simulation of Musculoskeletal Function in the Mouse Hindlimb During Trotting Locomotion. *Frontiers in Bioengineering and Biotechnology*, 6.

Charles, J. P., Cappellari, O., Spence, A. J., Hutchinson, J. R., and Wells, D. J. (2016a). Musculoskeletal Geometry, Muscle Architecture and Functional Specialisations of the Mouse Hindlimb. *PLOS ONE*, 11(4):e0147669.

Charles, J. P., Cappellari, O., Spence, A. J., Wells, D. J., and Hutchinson, J. R. (2016b). Muscle moment arms and sensitivity analysis of a mouse hindlimb musculoskeletal model. *Journal of Anatomy*, 229(4):514–535.

Danner, S. M., Shevtsova, N. A., Frigon, A., and Rybak, I. A. (2017). Computational modeling of spinal circuits controlling limb coordination and gaits in quadrupeds. *eLife*, 6:e31050.

Danner, S. M., Wilshin, S. D., Shevtsova, N. A., and Rybak, I. A. (2016). Central control of interlimb coordination and speed-dependent gait expression in quadrupeds. *J. Physiol.*, 594(23):6947–6967.

De Groote, F., Kinney, A. L., Rao, A. V., and Fregly, B. J. (2016). Evaluation of Direct Collocation Optimal Control Problem Formulations for Solving the Muscle Redundancy Problem. *Annals of Biomedical Engineering*, 44(10):2922–2936.

DeLaurier, A., Burton, N., Bennett, M., Baldock, R., Davidson, D., Mohun, T. J., and Logan, M. P. (2008). The Mouse Limb Anatomy Atlas: An interactive 3D tool for studying embryonic limb patterning. *BMC Developmental Biology*, 8(1):83.

Ekeberg, Ö. and Pearson, K. (2005). Computer Simulation of Stepping in the Hind Legs of the Cat: An Examination of Mechanisms Regulating the Stance-to-Swing Transition. *Journal of Neurophysiology*, 94(6):4256–4268.

Ermentrout, B. (1994). Reduction of Conductance-Based Models with Slow Synapses to Neural Nets. *Neural Computation*, 6(4):679–695.

Frigon, A., Akay, T., and Prilutsky, B. I. (2021). Control of mammalian locomotion by somatosensory feedback. *Comprehensive Physiology*, page 2877–2947.

Fujiki, S., Aoi, S., Tsuchiya, K., Danner, S. M., Rybak, I. A., and Yanagihara, D. (2019). Phase-dependent response to afferent stimulation during fictive locomotion: a computational modeling study. *Frontiers in Neuroscience*, 13:481553.

Geijtenbeek, T., van de Panne, M., and van der Stappen, A. F. (2013). Flexible muscle-based locomotion for bipedal creatures. *ACM Transactions on Graphics*, 32(6):1–11.

Gradwell, M. A., Ozeri-Engelhard, N., Eisdorfer, J. T., Laflamme, O. D., Gonzalez, M., Upadhyay, A., Medlock, L., Shrier, T., Patel, K. R., Aoki, A., Gandhi, M., Abbas-Zadeh, G., Oputa, O., Thackray, J. K., Ricci, M., George, A., Yusuf, N., Keating, J., Imtiaz, Z., Alomary, S. A., Bohic, M., Haas, M., Hernandez, Y., Prescott, S. A., Akay, T., and Abraira, V. E. (2024). Multimodal sensory control of motor performance by glycinergic interneurons of the mouse spinal cord deep dorsal horn. *Neuron*.

Guertin, P., Angel, M. J., Perreault, M. C., and McCrea, D. A. (1995). Ankle extensor group I afferents excite extensors throughout the hindlimb during fictive locomotion in the cat. *J. Physiol.*, 487(1):197–209.

Hansen, N., Akimoto, Y., and Baudis, P. (2019). CMA-ES/pycma.

Hansen, N. and Ostermeier, A. (2001). Completely Derandomized Self-Adaptation in Evolution Strategies. *Evolutionary Computation*, 9(2):159–195.

Hiebert, G. W., Whelan, P. J., Prochazka, A., and Pearson, K. G. (1996). Contribution of hind limb flexor muscle afferents to the timing of phase transitions in the cat step cycle. *J. Neurophysiol.*, 75(3):1126–1137.

Josset, N., Roussel, M., Lemieux, M., Lafrance-Zoubga, D., Rastqar, A., and Bretzner, F. (2018). Distinct contributions of mesencephalic locomotor region nuclei to locomotor control in the freely behaving mouse. *Current Biology*, 28(6):884–901.

Kiehn, O. (2016). Decoding the organization of spinal circuits that control locomotion. *Nature Reviews Neuroscience*, 17(4):224–238.

Kim, Y., Aoi, S., Fujiki, S., Danner, S. M., Markin, S. N., Ausborn, J., Rybak, I. A., Yanagihara, D., Senda, K., and Tsuchiya, K. (2022). Contribution of afferent feedback to adaptive hindlimb walking in cats: A neuromusculoskeletal modeling study. *Frontiers in Bioengineering and Biotechnology*, 10.

Laflamme, O. D., Markin, S. N., Deska-Gauthier, D., Banks, R., Zhang, Y., Danner, S. M., and Akay, T. (2023). Distinct roles of spinal commissural interneurons in transmission of contralateral sensory information. *Current Biology*, 33(16):3452–3464.e4.

Leiras, R., Cregg, J. M., and Kiehn, O. (2022). Brainstem circuits for locomotion. *Annual Review of Neuroscience*, 45(1):63–85.

Markin, S. N., Klishko, A. N., Shevtsova, N. A., Lemay, M. A., Prilutsky, B. I., and Rybak, I. A. (2010). Afferent control of locomotor CPG: Insights from a simple neuromechanical model: Afferent control of locomotor CPG. *Annals of the New York Academy of Sciences*, 1198(1):21–34.

Mayer, W. P., Murray, A. J., Brenner-Morton, S., Jessell, T. M., Tourtellotte, W. G., and Akay, T. (2018). Role of muscle spindle feedback in regulating muscle activity strength during walking at different speed in mice. *Journal of Neurophysiology*, 120(5):2484–2497.

McCrea, D. A. and Rybak, I. A. (2008). Organization of mammalian locomotor rhythm and pattern generation. *Brain Research Reviews*, 57(1):134–146.

Merel, J., Aldarondo, D., Marshall, J., Tassa, Y., Wayne, G., and Ölveczky, B. (2019). Deep neuroethology of a virtual rodent. *arXiv:1911.09451 [q-bio]*.

Paul, C., Bellotti, M., Jezernik, S., and Curt, A. (2005). Development of a human neuro-musculo-skeletal model for investigation of spinal cord injury. *Biological Cybernetics*, 93(3):153–170.

Pierrot-Deseilligny, E. and Burke, D. (2012). *The Circuitry of the Human Spinal Cord: Spinal and Corticospinal Mechanisms of Movement*. Cambridge University Press, New York, NY, 1st edition.

Prochazka, A. (1999). Quantifying proprioception. *Progress in Brain Research*, 123:133–142.

Prochazka, A. and Gorassini, M. (1998). Models of ensemble firing of muscle spindle afferents recorded during normal locomotion in cats. *The Journal of Physiology*, 507 (Pt 1):277–291.

Rossignol, S., Dubuc, R., and Gossard, J.-P. (2006). Dynamic sensorimotor interactions in locomotion. *Physiol. Rev.*, 86(1):89–154.

Ruder, L., Takeoka, A., and Arber, S. (2016). Long-distance descending spinal neurons ensure quadrupedal locomotor stability. *Neuron*, 92(5):1063–1078.

Rybak, I. A., Dougherty, K. J., and Shevtsova, N. A. (2015). Organization of the mammalian locomotor cpg: Review of computational model and circuit architectures based on genetically identified spinal interneurons. *eNeuro*, 2(5):ENEURO.0069–15.2015.

Saputra, A. A., Botzheim, J., Ijspeert, A. J., and Kubota, N. (2022). Combining Reflexes and External Sensory Information in a Neuromusculoskeletal Model to Control a Quadruped Robot. *IEEE Transactions on Cybernetics*, 52(8):7981–7994.

Saputra, A. A., Wei Hong, C., Ijspeert, A. J., and Kubota, N. (2020). A Muscle-Reflex Model of Forelimb and Hindlimb of Felidae Family of Animal with Dynamic Pattern Formation Stimuli. In *2020 International Joint Conference on Neural Networks (IJCNN)*, pages 1–8, Glasgow, United Kingdom. IEEE.

Schomburg, E., Petersen, N., Barajon, I., and Hultborn, H. (1998). Flexor reflex afferents reset the step cycle during fictive locomotion in the cat. *Experimental brain research*, 122:339–350.

Seth, A., Hicks, J. L., Uchida, T. K., Habib, A., Dembia, C. L., Dunne, J. J., Ong, C. F., DeMers, M. S., Rajagopal, A., Millard, M., Hamner, S. R., Arnold, E. M., Yong, J. R., Lakshmikanth, S. K., Sherman, M. A., Ku, J. P., and Delp, S. L. (2018). OpenSim: Simulating musculoskeletal dynamics and neuromuscular control to study human and animal movement. *PLOS Computational Biology*, 14(7):e1006223.

Shevtsova, N. A., Talpalar, A. E., Markin, S. N., Harris-Warrick, R. M., Kiehn, O., and Rybak, I. A. (2015). Organization of left–right coordination of neuronal activity in the mammalian spinal cord: Insights from computational modelling. *The Journal of Physiology*, 593(Pt 11):2403–2426.

Talpalar, A. E., Bouvier, J., Borgius, L., Fortin, G., Pierani, A., and Kiehn, O. (2013). Dual-mode operation of neuronal networks involved in left–right alternation. *Nature*, 500(7460):85–88.

Tata Ramalingasetty, S., Danner, S. M., Arreguit, J., Markin, S. N., Rodarie, D., Kathe, C., Courtine, G., Rybak, I. A., and Ijspeert, A. J. (2021). A Whole-Body Musculoskeletal Model of the Mouse. *IEEE Access*, 9:163861–163881.

Todorov, E., Erez, T., and Tassa, Y. (2012). MuJoCo: A physics engine for model-based control. In *2012 IEEE/RSJ International Conference on Intelligent Robots and Systems*, pages 5026–5033.

Toeda, M., Aoi, S., Fujiki, S., Funato, T., Tsuchiya, K., and Yanagihara, D. (2020). Gait Generation and Its Energy Efficiency Based on Rat Neuromusculoskeletal Model. *Frontiers in Neuroscience*, 13.

Whelan, P. J., Hiebert, G. W., and Pearson, K. G. (1995). Stimulation of the group I extensor afferents prolongs the stance phase in walking cats. *Exp. Brain Res.*, 103(1):20–30.

Whelan, P. J. and Pearson, K. G. (1997). Comparison of the effects of stimulating extensor group I afferents on cycle period during walking in conscious and decerebrate cats. *Exp. Brain Res.*, 117(3):444–452.

Yakovenko, S. (2011). *A hierarchical perspective on rhythm generation for locomotor control*, page 151–166. Elsevier.

Zhang, H., Shevtsova, N. A., Deska-Gauthier, D., Mackay, C., Dougherty, K. J., Danner, S. M., Zhang, Y., and Rybak, I. A. (2022). The role of V3 neurons in speed-dependent interlimb coordination during locomotion in mice. *eLife*, 11:e73424.